Electrical properties of InAs1-xSbx and InSb nanowires grown by molecular beam epitaxy

C. Thelander, P. Caroff, S.R. Plissard, K.A. Dick

Applied Physics Letters

Electrical properties of $InAs_{1-x}Sb_x$ and InSb nanowires grown by molecular beam epitaxy

Cite as: Appl. Phys. Lett. **100**, 232105 (2012); https://doi.org/10.1063/1.4726037
Submitted: 19 February 2012 • Accepted: 18 May 2012 • Published Online: 06 June 2012

Claes Thelander, Philippe Caroff, Sébastien Plissard, et al.

AIP Publishing

Electrical properties of $InAs_{1-x}Sb_x$ and InSb nanowires grown by molecular beam epitaxy

Claes Thelander,[1,a)] Philippe Caroff,[2] Sébastien Plissard,[3,b)] and Kimberly A. Dick[1,4]
[1]*Solid State Physics, Lund University, Box 118, S-221 00 Lund, Sweden*
[2]*Institut d'Electronique, de Microélectronique et de Nanotechnologie, UMR CNRS 8520, Avenue Poincaré, B.P. 60069, 59652 Villeneuve d'Ascq, France*
[3]*Department of Applied Physics, Photonics and Semiconductor Nanophysics, Eindhoven University of Technology, P.O. Box 513, NL-5600 MB Eindhoven, The Netherlands*
[4]*Polymer & Materials Chemistry, Lund University, Box 124, S-221 00 Lund, Sweden*

(Received 19 February 2012; accepted 18 May 2012; published online 6 June 2012)

Results of electrical characterization of Au nucleated $InAs_{1-x}Sb_x$ nanowires grown by molecular beam epitaxy are reported. An almost doubling of the extracted field effect mobility compared to reference InAs nanowires is observed for a Sb content of $x = 0.13$. Pure InSb nanowires on the other hand show considerably lower, and strongly diameter dependent, mobility values. Finally, InAs of wurtzite crystal phase overgrown with an $InAs_{1-x}Sb_x$ shell is found to have a substantial positive shift in threshold voltage compared to reference nanowires. © *2012 American Institute of Physics*. [http://dx.doi.org/10.1063/1.4726037]

$InAs_{1-x}Sb_x$ has a direct bandgap that is the narrowest among the III-V semiconductors (145 meV for $x = 0.63$ at 0 K), with absorption wavelengths in the mid infrared (3–12 μm), a range important for atmospheric gas sensing.[1] Due to a very high carrier mobility, the material is also investigated in the development of high-electron mobility transistors (HEMTs)[2] and hetero-junction bipolar transistors (HBTs).[3] However, growth of $InAs_{1-x}Sb_x$ materials is complicated from a material perspective, and optimized buffer layers are required for each desired As/Sb composition.[4] An alternative to forming $InAs_{1-x}Sb_x$ layer-by-layer is to grow the material in the shape of nanowires, where epitaxial and dislocation-free materials with various As/Sb compositions can be formed on the same starting substrate.[5–7] Nanowires of binary InAs and InSb are currently studied very intensely in research related to quantum computation, motivated by the strong spin-orbit interaction in InAs and InSb, which simplifies spin manipulation,[8–10] and the observation of new quasiparticles, such as Majorana fermions.[11] Access to ternary $InAs_{1-x}Sb_x$ material will likely offer a possibility to tune important material-related properties, such as spin-orbit coupling and quantum confinement.

In this Letter, we report on the electrical properties of Au-seeded $InAs_{1-x}Sb_x$ nanowires grown by molecular beam epitaxy (MBE). InAs ($x = 0$) is a well studied nanowire material in terms of structural and electrical properties[12–14] and was used as reference. In the opposite composition range ($x = 1$), the results were also compared to measurements on pure InSb nanowires grown by the same technique. The Sb-containing nanowires were all nucleated from InAs stems[7,15] with a wurtzite (WZ) crystal structure, which changed to zinc-blende (ZB) upon introduction of a sufficient level of Sb.[5,16] Typically, both segments overgrow radially, thus also providing an Sb-containing shell around the WZ InAs base.

Compared to reference InAs nanowires, we find that a small level of Sb incorporation ($x = 0.13$) leads to a considerably increased field-effect mobility for the ZB segments, as well as an overall higher mobility for the overgrown WZ base segments. On the other hand, for binary InSb nanowires within a diameter range of 50–100 nm, very low mobility values were observed, consistent with recent reports.[17–19] However, we find the mobility to be strongly diameter dependent, such that nanowires in the low diameter range had very high resistivity and low extracted mobility, whereas thicker wires show improved values.

The nanowire samples were grown by gas source-MBE on InP(111)B substrates via a standard gold seed-assisted mechanism at 410 °C. Gold seeds were obtained during a 3 min annealing/deoxidation step at 510 °C, by dewetting of a 3 Å thick gold film. All nanowires in this work were grown on top of short InP stems to facilitate vertical nucleation.[14] InAs nanowires [sample A, Fig. 1(a)] with pure WZ crystal phase were grown under 2D layer equivalent V/III ratios in the range of 2–2.5 and cooled-down under As_2 flux.

Sample B [Fig. 1(b)] was grown to nominally have two axial segments: InAs, grown for 25 min, at the bottom and $InAs_{1-x}Sb_x$, grown for 20 min, at the top, followed by cool-down under vacuum conditions only. The top $InAs_{1-x}Sb_x$ segment was grown by opening the shutter of an antimony valved cracker cell, where the Sb flux was set to a GaSb(001) 2D group V equivalent growth rate of 0.2 ML/s. The bottom WZ InAs nanowire segment became completely overgrown with a WZ $InAs_{1-x}Sb_x$ shell during growth of the top axial InAsSb segment, which is pure ZB as shown in Figs. 1(h) and 1(i) by high resolution transmission electron microscopy (TEM) [see also Ref. 16]. The nanowires on sample B thus have two $InAs_{1-x}Sb_x$ segments, with different crystal structure and radial composition. For this sample, x-ray energy dispersive spectroscopy (XEDS) operated in scanning TEM mode showed that the top (ZB) $InAs_{1-x}Sb_x$ segment has a

a)Electronic mail: claes.thelander@ftf.lth.se.
b)This research was performed while S. Plissard was at Institut d'Electronique, de Microélectronique et de Nanotechnologie, UMR CNRS 8520, Avenue Poincaré, B.P. 60069, 59652 Villeneuve d'Ascq, France.

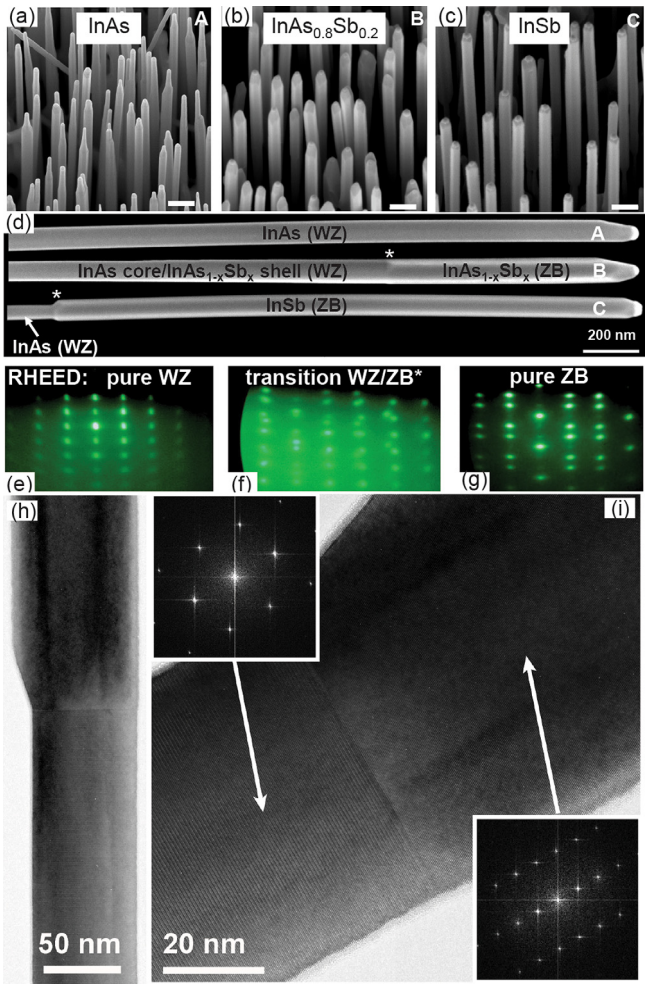

FIG. 1. (a)-(c) Overview SEMs of as-grown InAs, $InAs_{1-x}Sb_x$, and InSb samples listed in Table I after MBE growth. Scale bars: 200 nm (d) close-up SEMs of representative InAs, $InAs_{1-x}Sb_x$, and InSb nanowires. (e)-(g) RHEED pattern obtained *in-situ* during growth of the InAs segment (e), shortly after beginning the growth of the InSb (f), and during the growth of the InSb segment (g). In all cases, the electron beam was perpendicular to the {1-10}//{11-20} planes and gives a signal from approximately the upper 100 nm of the nanowires. The patterns in (e) and (g) are characteristic of WZ and ZB (consisting of an ensemble of wires in two possible ZB orientations), respectively, while (f) is a combination of the two. (h) TEM image of the interface region of an InAs-$InAs_{1-x}Sb_x$ nanowire illustrating that the structure is free of stacking defects. The growth direction is up in the image. (i) High resolution TEM image of the interface region of the nanowire in (h), showing that the lower InAs region is pure WZ while the upper $InAs_{1-x}Sb_x$ region is pure ZB. The inset fast Fourier transforms confirm the two crystal structures.

core (axial) composition of $x = 0.09$ and shell (radial overgrowth) composition of $x = 0.21$, with an average segment composition of $x = 0.13 \pm 0.015$ measured over 30 nanowires. The bottom (WZ) segment, which is pure InAs at the core, has a measured shell composition of about $x = 0.16$ and average composition of about $x = 0.09$.

Finally, sample C [Fig. 1(c)] consists of an InAs/InSb nanowire heterostructure, where the ZB InSb was grown on top of a WZ InAs stem, similar to the procedure used for sample B. The Sb flux was set to a GaSb(001) 2D equivalent growth rate of 2.5 ML/s. In contrast to sample B, sample C does not show any lateral overgrowth of the bottom InAs segment [Fig. 1(d)], in accordance with previous reports on this nanowire heterostructure grown by metalorganic vapour phase epitaxy.[7] The evolution of the crystal structure from WZ to ZB along the nanowire axis was monitored *in-situ* by reflection high energy electron diffraction (RHEED), as illustrated by the three consecutive diffraction patterns shown in Figs. 1(e)–1(g).

For electrical characterization, nanowires were mechanically transferred to degenerately doped Si samples with a 100 nm SiO_2 insulating surface layer. Scanning electron microscopy (SEM) inspection was carried out at low magnification to record the position of nanowires. Contacts were fabricated by electron beam lithography, followed by oxygen plasma ashing, and etching in $(NH_4)_2S_x$ and H_2O 1:9 at 40 °C for 1–2 min. A layer of 25 nm Ni and 75 nm Au was evaporated onto the samples in the lift-off process. Electrical measurements were carried out in a dark, evacuated chamber at room-temperature. Detailed SEM inspection was made after electrical characterization, where nanowire diameter, D, was obtained by averaging the diameter of a nanowire over its free length, L, between the contacts. The samples were designed such that L was in the range 550–600 nm. Values for the nanowire resistivity, ρ, were obtained by approximating the nanowires with a cylindrical geometry, $\rho = R\pi D^2/4L$, where R is the nanowire resistance.

The threshold voltage, V_T, for each device was extracted from the transfer characteristics (I-V_G) by linear extrapolation from the point of highest transconductance, g, to the intercept with the gate voltage (V_G) axis for $I = 0$. Finally, values for room-temperature field-effect mobility, μ, were estimated from $\mu = gL^2/(C_G V_D)$, where g is the transconductance in the linear regime, V_D the applied drain voltage (10 mV), and C_G the nanowire to back-gate capacitance obtained from $C_G = 2\pi\varepsilon_0\varepsilon_{r,eff}L/\ln(4t/D + 2)$, using $t = 100$ nm (thickness of SiO_2) and $\varepsilon_{r,eff} = 2.2$.[20] The values for g and μ were in all cases obtained by averaging over a V_G range of 1.4 V.

Reference InAs nanowires of WZ crystal structure show n-type depletion mode transfer (I-V_G) characteristics, with a threshold voltage, V_T, of −5.4 V (Fig. 2(a)). This is consistent with earlier reports on the transport properties of such nanowires,[12] where the high carrier density at $V_G = 0$ V is explained in part by a surface pinning of the Fermi level in the conduction band of InAs.

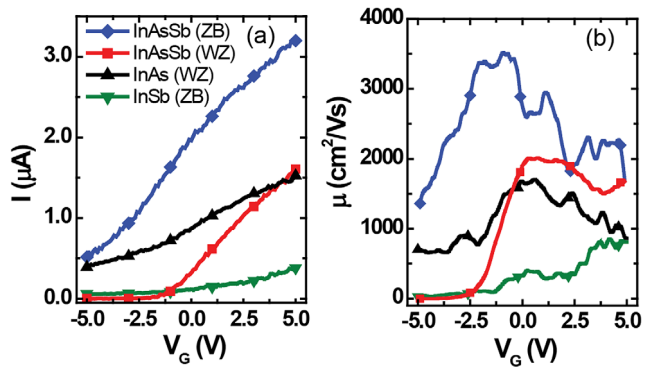

FIG. 2. Electrical measurements ($V_D = 10$ mV and $T = 295$ K) for nanowires of different composition and crystal structures, but with similar device dimensions ($D = 70 \pm 3$ nm, $L_G = 570 \pm 30$ nm). (a) I-V_G sweep. (b) Field-effect mobility (μ) vs. V_G extracted from (a).

$InAs_{1-x}Sb_x$ nanowires, with a WZ base and a ZB top, were processed with pairs of electrodes to each of the two segments. Four-probe measurements of such nanowires indicated vanishingly small contact resistance compared to the overall device resistance. Both segments showed higher values for g and μ compared to InAs reference wires (sample A) with similar gate length and diameter (Table I). The WZ $InAs_{1-x}Sb_x$ segments had considerably higher average $V_T = -0.6$ V compared to the corresponding ZB segments (−5.8 V) and the reference WZ InAs nanowires (−5.4 V). This shows that the carrier concentration in the case of the WZ $InAs_{1-x}Sb_x$ nanowires is strongly reduced. An average change in V_T with +5 V (Table I) corresponds to approximately 10^3 electrons for $C_G = 32$ aF, which is a decrease in carrier concentration by 5×10^{17} cm^{-3} using an average nanowire volume between source and drain.

Pure InSb nanowires of ZB crystal structure from sample C showed high values for the resistivity, and also low transconductance [Fig. 2(a)]. However, the electrical properties depend very strongly on nanowire diameter, as seen in Fig. 3. The thinnest nanowires (50–60 nm) had positive $V_T = 1.8$ V, whereas the thickest nanowires studied (95–100 nm) had $V_T = -0.1$ V. The peak in the extracted room-temperature field-effect mobility (μ_{peak}) was only 450 cm^2/Vs for the thinner nanowires, but increased up to 1000 cm^2/Vs for the thickest nanowires. However, due to the positive V_T shift compared to the other materials in Table I, it is possible that the true maximum in transconductance is not always reached at $V_G = +5$ V for the thinner InSb nanowires in the study. These mobility values are very far from the bulk values for InSb, but shows that further improvement can be expected for material with even higher volume-to-surface ratio, or for nanowires with a passivating surface layer. A second sample was fabricated with a range of contact separations to elucidate whether a high contact resistance limits the transconductance. For nanowires in the diameter range of 90–100 nm, no drop in device resistivity was found when doubling the source-drain distance to extend over the total length of the InSb segments (1000–1100 nm). This indicates that the transconductance was not primarily limited by contact resistance, but by scattering in the nanowire, likely associated with surface states and charges trapped at the surface.

The observation of a strong diameter dependence of the mobility of InSb nanowires fits well with results reported from earlier studies. Wang *et al*. studied thin (30–50 nm diameter) ⟨110⟩-oriented InSb nanowires grown by pulsed laser CVD and extracted very low mobility values in the range 100–130 cm^2/Vs.[17] Transport in thick (100 nm), tapered InSb nanowires grown by electro deposition was investigated by Das *et al*., who found field-effect mobility values around 1200 cm^2/Vs.[18] Our findings also agree with observations based on InAs nanowires, where a similar mobility degradation of unpassivated nanowires is observed for thin wires.[13] However, for InAs, the onset of mobility degradation occurs for smaller diameters (30–40 nm), which may be related to the reduced Bohr exciton radius and quantum confinement in that material compared to InSb.

Preliminary results on ZB $InAs_{1-x}Sb_x$ with higher Sb contents ($x \sim 0.28$) showed very low values for the resistivity ($\rho = 2.3$ mΩ cm) at $V_G = 0$. At the same time, the extracted mobility was found to be reduced for this growth ($\mu_{peak} = 1520$ cm^2/Vs), which points to a high carrier concentration ($n = 1$–2×10^{18} cm^{-3}). However, the results are not conclusive, since the nanowires on average were considerably thicker ($D = 105$ nm). Still the data suggest that there should be an abrupt transition in the electrical properties for sufficiently high Sb content, going from $InAs_{1-x}Sb_x$ material with a very high carrier concentration to InSb with very low carrier concentration. This is likely related to a difference in surface Fermi level pinning position relative to the conduction band edge of InAs and InSb, possibly linked to band bowing, where a conduction band edge minimum is predicted for $x = 0.26$.[21] Ordering during epitaxial growth has been shown to give rise to a reduced bandgap for InAsSb materials,[22] although TEM inspections showed no such indications in the material studied here.

It is interesting that the $InAs_{1-x}Sb_x$ overgrowing the WZ InAs stem effectively reduces the nanowire carrier concentration. This may have several causes, such as a shift in Fermi level pinning position for WZ material relative to ZB, strain due to the shell,[21] or that WZ $InAs_{1-x}Sb_x$ would have an opposite conduction band offset to InAs compared to the case of ZB. For transistor applications, this observation is particularly important as it offers an original means to shift V_T.

In conclusion, the electrical properties of ternary $InAs_{1-x}Sb_x$ and binary InAs and InSb nanowires grown by MBE were studied and compared. For similar device geometries, we find the $InAs_{1-x}Sb_x$ material to have higher transconductance and field-effect mobility. Radial overgrowth of WZ InAs with $InAs_{1-x}Sb_x$ gave a considerably reduced carrier concentration. Binary InSb nanowires show low extracted values for field-effect mobility, although with a strong diameter dependence. It is suggested that passivating schemes will be required to reach higher room temperature mobilities in Sb-based nanowires. The results show the relevance of further development of axial and radial composition tuning of narrow band gap nanowires to optimize the electrical properties.

TABLE I. Averaged data of nanowire samples included in the study.

Sample	Material	Crystal phase	NWs	D (nm)	L_G (nm)	$C_{G,model}$ (aF)	ρ (mΩ cm)	V_T (V)	μ_{peak} (cm^2/Vs)
A	InAs	WZ	7	67	580	33	8.1	−5.4	1560
B	$InAs_{0.91}Sb_{0.09}$	WZ	6	68	550	32	50	−0.6	2410
B	$InAs_{0.87}Sb_{0.13}$	ZB	6	72	550	33	4.1	−5.8	3410
C	InSb	ZB	2	56	590	31	93	1.8	450
C	InSb	ZB	3	74	600	36	66	1.1	760
C	InSb	ZB	4	98	580	39	45	−0.1	1010

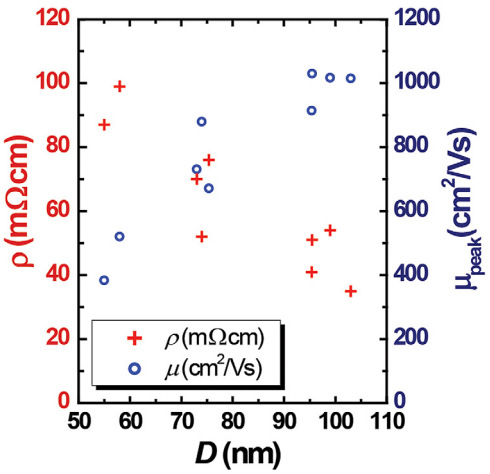

FIG. 3. Resistivity and extracted μ_{peak} for InSb nanowires plotted as a function of studied nanowire diameter. L_G is constant = 590 ± 10 nm.

This work received financial support from the Nanometer Structure Consortium at Lund University (nmC@LU), the Swedish Research Council (VR), the Swedish Foundation for Strategic Research (SSF), and the Knut and Alice Wallenberg Foundation (KAW). It also received financial support from the French National Research Agency (ANR), TERADOT project, under Contract No.ANR-11-JS04-002-01.

[1]M. Y. Yen, R. People, K. W. Wecht, and A. Y. Cho, Appl. Phys. Lett. **52**, 489 (1988).
[2]J. B. Boos, W. Kruppa, B. R. Bennett, D. Park, S. W. Kirchoefer, R. Bass, and H. B. Dietrich, IEEE Trans. Electron Devices **45**, 1869 (1998).
[3]J. G. Champlain, R. Magno, R. Bass, D. Park, and J. B. Boos, Electron. Lett. **46**, 1333 (2010).
[4]B.-R. Wu, C. Liao, and K. Y. Cheng, Appl. Phys. Lett. **92**, 062111 (2008).
[5]B. M. Borg, K. A. Dick, J. Eymery, and L.-E. Wernersson, Appl. Phys. Lett. **98**, 113104 (2011).
[6]D. Ercolani, M. Gemmi, L. Nasi, F. Rossi, M. Pea1, A. Li, G. Salviati, F. Beltram, and L. Sorba, Nanotechnology **23**, 115606 (2012).
[7]P. Caroff, J. B. Wagner, K. A. Dick, H. A. Nilsson, M. Jeppsson, K. Deppert, L. Samuelson, L. R. Wallenberg, and L.-E. Wernersson, Small **4**, 878 (2008).
[8]S. Csonka, L. Hofstetter, F. Freitag, S. Oberholzer, C. Schonenberger, T. S. Jespersen, M. Aagesen, and J. Nygård, Nano Lett. **8**, 3932 (2008).
[9]H. A. Nilsson, P. Caroff, C. Thelander, M. Larsson, J. B. Wagner, L.-E. Wernersson, L. Samuelson, and H. Q. Xu, Nano Lett. **9**, 3151 (2009).
[10]S. Nadj-Perge, S. M. Frolov, E. P. A. M. Bakkers, and L. P. Kouwenhoven, Nature (London) **468**, 1084 (2010).
[11]V. Mourik, K. Zuo, S. M. Frolov, S. R. Plissard, E. P. A. M. Bakkers, and L. P. Kouwenhoven, Science **336**, 1003 (2012).
[12]C. Thelander, K. A. Dick, M. T. Borgstrom, L. E. Froberg, P. Caroff, H. A. Nilsson, and L. Samuelson, Nanotechnology **21**, 205703 (2010).
[13]M. Scheffler, S. Nadj-Perge, L. P. Kouwenhoven, M. T. Borgström, and E. P. A. M. Bakkers, J. Appl. Phys. **106**, 124303 (2009).
[14]C. Thelander, P. Caroff, S. Plissard, A. W. Dey, and K. A. Dick, Nano Lett. **11**, 2424 (2011).
[15]L. Lugani, D. Ercolani, F. Rossi, G. Salviati, F. Beltram, and L. Sorba, Cryst. Growth. Des. **10**, 4038 (2010).
[16]T. Xu, K. A. Dick, S. Plissard, T. H. Nguyen, Y. Makoudi, M. Berthe, J.-P. Nys, X. Wallart, B. Grandidier, and P. Caroff, Nanotechnology **23**, 095702 (2012).
[17]Y. Wang, J. Chi, K. Banerjee, D. Grutzmacher, T. Schapers, and J. G. Lu, J. Mater. Chem. **21**, 2459 (2011).
[18]S. R. Das, C. J. Delker, D. Zakharov, Y. P. Chen, T. D. Sands, and D. B. Janes, Appl. Phys. Lett. **98**, 243504 (2011).
[19]H. A. Nilsson, P. Caroff, C. Thelander, E. Lind, O. Karlstrom, and L.-E. Wernersson, Appl. Phys. Lett. **96**, 153505 (2010).
[20]O. Wunnicke, Appl. Phys. Lett. **89**, 083102 (2006).
[21]S.-H. Wei and A. Zunger, Phys. Rev. B. **52**, 12039 (1995).
[22]S. R. Kurtz, L. R. Dawson, R. M. Biefeld, D. M. Follstaedt, and B. L. Doyle, Phys. Rev. B **46**, 1909 (1992).